Piecewise Polynomial Modeling for Control and Analysis of Aircraft Dynamics beyond Stall

Torbjørn Cunis, Laurent Burlion, Jean-Philippe Condomines

Piecewise Polynomial Modeling for Control and Analysis of Aircraft Dynamics beyond Stall

Torbjørn Cunis* and Laurent Burlion†
ONERA – The French Aerospace Lab, Centre Midi-Pyrénées, Toulouse, 31055, France

Jean-Philippe Condomines‡
French Civil Aviation School, Toulouse, 31055, France

Nomenclature

α_0 = Low-angle of attack boundary (°);

ρ = Pseudo-radius ($\rho \in \mathbb{R}$);

$\varphi(\cdot)$ = Boundary condition function ($\varphi\colon \mathbb{R}^m \to \mathbb{R}$);

Σ = Positive-definite shape factor ($\Sigma \in \mathbb{R}^{n\times n}$);

Ω_φ = Boundary curve set ($\Omega_\phi \subset \mathbb{R}^m$);

$C_{\mathrm{l,m,n}}$ = Aerodynamic coefficients of moments in body axes $(\cdot)$;

$C_{\mathrm{X,Y,Z}}$ = Aerodynamic coefficients of forces in body axes $(\cdot)$;

$\mathbf{C}$ = Objective matrix ($\mathbf{C} \in \mathbb{R}^{k\times r}$);

$\mathbf{d}$ = Vector of measurements ($\mathbf{d} \in \mathbb{R}^k$);

$\mathbf{f}(\cdot)$ = Non-linear, open-loop system dynamics ($\mathbf{f}\colon (\mathbf{X}, \cdot) \mapsto \dot{\mathbf{X}}$);

$g(\cdot), h(\cdot)$ = Positive-semi-definite Lagrange multiplier ($g, h\colon \mathbb{R}^n \to \mathbb{R}_{\geq 0}$);

k = Number of measurements;

m = Number of variables;

n = Number of states; system degree; polynomial degree;

$\mathbf{q}$ = Vector of coefficients ($\mathbf{q} \in \mathbb{R}^r$);

r = Number of coefficients;

*Doctoral Researcher, Department of Information Processing and Systems, e-mail: torbjoern.cunis@onera.fr; associated researcher with the French Civil Aviation School, Drones Research Group; AIAA Student Member.

†Research Scientist, Department of Information Processing and Systems, e-mail: laurent.burlion@onera.fr.

‡Assistant Professor, Drones Research Group, e-mail: jean-philippe.condomines@enac.fr.

$\mathbf{X}^*, \boldsymbol{\mu}^*$ = States and parameters at trim condition;

$(\cdot)^{post}$ = Domain of high angle of attack;

$(\cdot)^{pre}$ = Domain of low angle of attack;

$\mathcal{X}$ = State space ($\mathcal{X} \subseteq \mathbb{R}^n$);

$\partial\mathcal{X}$ = Set boundary of $\mathcal{X}$.

I. Introduction

FULL-ENVELOPE aircraft models require extensive effort to represent the aerodynamic coefficients well in the entire region of the envelope as flight dynamics beyond stall are highly non-linear and often unstable [1, 2]. With upset recovery approaches found in the literature being model-based ([3–5], and references herein) there is a clear need for reliable full-envelope models of flight dynamics. NASA's *Generic Transport Model* (GTM) has contributed significantly to analysis and control approaches of civil and unmanned aircraft over the entire flight envelope (see, e.g., [6, 7]). Representing a 5.5 % down-scaled typical aerial transport vehicle, the GTM provides exhaustive, full-envelope aerodynamic data from wind-tunnel studies [8] and its open-source aerodynamic model for MATLAB/Simulink [9] has given access for development of modeling, analysis, and control methods to the aerospace community. An overview of research studies on longitudinal trim conditions, regions of attraction, and upset situations can be found in [2, 5, 10, 11]. However, analytical representations proposed for the full-envelope aerodynamics are still insufficient for non-linear analysis and control design [12]. Therefore, improved methods for accurate modeling are imperative, in particular when developing robust and powerful advanced control strategies for upset recovery. Subsequently, model feedback designs based on full-envelope aerodynamic models will grant full authority and control efficiency for stability and performances in unmanned aircraft (UA) [13].

Polynomial models of the aerodynamic coefficients have provided a constructive method to define and evaluate models based on analytical computation due to their continuous and differentiable nature. Despite the fact that polynomial models have been published recently [10, 11], none of the results represent the aerodynamic coefficients well in the entire region of the envelope [12]. Indeed, at the stall angle of attack, the laminar flow around the wings in the pre-stall region changes to turbulent flow and remains so in post-stall. This significant change of the flow dynamics motivates a piecewise model of the pre-stall and post-stall dynamics instead.

Piecewise regression theory can be dated to the 1970s; first research focused on regression of a few polynomial functions piecewise over the observations. However, the estimation of suitable switching surfaces

or *joints* for the piecewise functions usually adds computational difficulty and load [14–17]. Later, *multivariate splines* were introduced [18, 19]; using simplices and baryocentric coordinates for the base, the so-called B-splines bear the advantage of generalized continuity, dimensional flexibility, and efficient evaluation as well as a stable local basis [20]. Recently, a further approach combining splines with fuzzy logic has been presented in [21].

While splines today present a powerful yet complex tool for accurate and smooth interpolation, they lack an underlying physical model justifying the partition. Moreover, for functional analysis of trim conditions and stable sets, as in [10, 11], splines weren't used but polynomials. Motivated by the practical problems encountered with mini-UAs flight control and guidance, civil aircraft fault detection and isolation, and upset recovery, we aim to derive a simple yet powerful aerodynamic model still suitable for functional analysis. A novel approach for piecewise polynomial modeling aerodynamic coefficients, the `pwpfit` toolbox for MATLAB, was recently proposed in [22]. Here, we have proven feasibility of fitting both a piecewise polynomial model and its joint surface using *linear least-square* (LSQ) optimization techniques. While this approach is limited to a single joint without differential continuity, the switch in the dynamics is motivated by the change from laminar to turbulent flow at stall and the resulting model is found to fit the full-envelope aerodynamics well.

This article focuses on the recent research detailing the theoretical aspects in the sequel and their application to functional analysis. The main contributions of this paper are therefore: to address (in §II) a concise bibliographical review of the polynomial based-methods used for full-envelope identification; to introduce (in §III) a novel and generic formulation of the piecewise polynomial fitting method which approximates a piecewise polynomial function and its joint; to provide (in §IV) a six-degrees-of-freedom model of an aircraft and its aerodynamic coefficients, accounting for both pre-stall and post-stall characteristics by piecewise identification; and finally to demonstrate and assess the extension of functional analysis tools for the piecewise polynomial model (in §V).

II. State of the Art

A. Polynomial regression

Polynomial regression is a general approach similar to linear curve regression, where a polynomial function f is to be found in order to approximate best a set of measured data points. Here, the coefficients of f are subject to the optimality problem of minimal sum of squared residuals of f with respect to the measurements (*goodness of fit*, GoF). The formulation of optimal coefficients as a linear least-square problem dates back to Legendre (1805) and Gauss (1809); a first application can be found by Gergonne in 1815 [23]. It has been shown that on average, the residuals of such an optimal polynomial vanish and their deviation is

minimized [24]. Furthermore, polynomial functions are defined by basic mathematical operations of addition and multiplication and thus provide by their nature smoothness to infinite differentiation. Recent polynomial models of the full-envelope aerodynamic coefficients of the GTM have been presented in [10, 11].

B. Multi-variate splines

Splines are piecewise sequences of polynomial functions, where each polynomial is active only in the respective partition. These partitions are chosen before fitting instead of being subject of the fit. The polynomials sub-functions are computed such that at the boundaries of the selected partitions the overall spline function is smooth to a certain degree of continuity. Thus, spline functions show characteristics of both lookup tables and polynomials, as noted by de Visser et al. [18, p. 3]:

> Effectively, spline functions [...] combine the global nonlinear modeling capability of lookup tables with the analytic, continuous nature of polynomials.

While for a single-variable spline function, the boundaries equal point-wise joints, the partitions of multi-variate splines can be more complex. In addition to simple rectangles (or rather rectangular polytopes), triangular partitions have recently proposed by [20]. However, the high accuracy of splines in terms of their residuals is opposed by their computational costs for further analytical investigation. Multi-variate splines have been used in, among others, [18, 19] in order to model full-envelope aerodynamics.

III. Methodology

In vector notation, optimal coefficients for piecewise polynomial fits are expressed as linear least-squares. We introduce a polynomial notation by the vectors of monomials and coefficients and thus reduce the goodness of fit to a function of the latter. The joint will be given by the scalar field $\varphi(\cdot)$ in the variables of the model and the scalar bound x_0; here, we assume φ to be linear matrix inequality and x_0 will be determined by the fitting. The resulting model then has a single joint with value continuity, i.e., the model is not differentiable at the joint. For models in several variables and outputs, such as the aerodynamic coefficients, it is desirable to have further constraints to the fit enforced. We will add those desired properties of the piecewise fit as constraint matrices.

Definition 1 A *linear least-square* (LSQ) problem is given as the optimization problem

$$\mathrm{lsq}(\mathbf{C}, \mathbf{d}, \mathbf{A}, \mathbf{0}) = \arg\min_{\mathbf{q}\in\Omega_{\mathbf{A}}} \|\mathbf{C}\mathbf{q} - \mathbf{d}\|_2^2 \,. \tag{1}$$

with $\mathbf{q} \in \mathbb{R}^r$, $\mathbf{C} \in \mathbb{R}^{k\times r}$, $\mathbf{d} \in \mathbb{R}^k$, and $\Omega_{\mathbf{A}} = \{\mathbf{q} \,|\mathbf{A}\mathbf{q} = \mathbf{0}\}$ for a constraint matrix $\mathbf{A}$.

A. Polynomials

A *monomial of degree n* is a single product of powers where the exponents add up to the total degree n, without any scalar coefficient. We notate a monomial of $\mathbf{x} = (x_1, \ldots, x_m)$ in degrees $\mathbf{n} = (n_1, \ldots, n_m)$ as

$$\mathbf{x}^{\mathbf{n}} = x_1^{n_1} \ldots x_m^{n_m}, \tag{2}$$

where $\mathbf{x}^{\mathbf{n}}$ has the total degree $n = \|\mathbf{n}\|_1 = n_1 + \cdots + n_m$.

Definition 2 $\boldsymbol{\mathcal{P}}_n(\mathbf{x})$ is the *vector of monomials* $\mathbf{x}^{\boldsymbol{\nu}}$ in variables $\mathbf{x} = (x_1, \ldots, x_m)$ with degrees $\boldsymbol{\nu} \in \mathbb{N}^m$ and total degrees $\|\boldsymbol{\nu}\|_1 \leq n$; and the number of elements in $\boldsymbol{\mathcal{P}}_n(\mathbf{x})$ is denoted by $\mathfrak{r}[n]$, i.e., $\boldsymbol{\mathcal{P}}_n \in \mathbb{R}\left[\mathbf{x}\right]^{\mathfrak{r}[n]}$.

By this notation, a polynomial f is expressed as scalar product of its monomials and coefficients,

$$f(\mathbf{x}) = \langle \boldsymbol{\mathcal{P}}_n(\mathbf{x}), \mathbf{q} \rangle \tag{3}$$

with the *vector of coefficients* $\mathbf{q} \in \mathbb{R}^{\mathfrak{r}[n]}$.

B. Piecewise polynomial fitting

Consider the k observations $(\mathbf{x}_i, z_i)_i$ given as sequences over $i \in [1, k]$:

$$z_i = \gamma(\mathbf{x}_i) + \epsilon_i, \tag{4}$$

where $(\mathbf{x}_i, z_i, \epsilon_i)_{1 \leq i \leq k} \subset \mathbb{R}^m \times \mathbb{R} \times \mathbb{R}$ and $\gamma(\cdot)$ and $(\epsilon_i)_i$ are an unknown function and measurement error, respectively; we will find coefficients $\mathbf{q}_1, \mathbf{q}_2$ as well as a scalar $x_0 \in \mathbb{R}$ such that

$$f : \mathbf{x} \longmapsto \begin{cases} \langle \boldsymbol{\mathcal{P}}_n(\mathbf{x}), \mathbf{q}_1 \rangle & \text{if } \varphi(\mathbf{x}) \leq x_0; \\ \langle \boldsymbol{\mathcal{P}}_n(\mathbf{x}), \mathbf{q}_2 \rangle & \text{else;} \end{cases}$$

with $\varphi : \mathbb{R}^m \to \mathbb{R}$ minimizes the sum of squared residuals

$$\mathrm{GoF}(f) =_{\mathrm{def}} \sum_{i=1}^{k} |f(\mathbf{x}_i) - z_i|^2 \tag{5}$$

for an $n > 0$. We note the sub-polynomials of f by $f_{1,2} : \mathcal{X}_{1,2} \to \mathbb{R}, \mathbf{x} \mapsto \langle \boldsymbol{\mathcal{P}}_n(\mathbf{x}), \mathbf{q}_{1,2} \rangle$ with $\mathcal{X}_1 \cap \mathcal{X}_2 = \varnothing$ and call $\mathcal{X}_1 \cup \mathcal{X}_2$ the *entire domain of* f. The *joint* of f is given by $\Omega_\varphi =_{\mathrm{def}} \partial\mathcal{X}_1 \cap \partial\mathcal{X}_2 = \{\mathbf{x} \,|\varphi(\mathbf{x}) = x_0\}$; if $\varphi(\cdot)$ is a linear matrix inequality, the boundary is convex. Re-writing the goodness of fit using matrix calculus, we reduce the cost functional to a cost function and polynomial data fitting to a linear least-square problem.

The cost functional for f can be evaluated piecewise to

$$\mathrm{GoF}(f) = \sum_{\mathbf{x}_i \in X_1} |f_1(\mathbf{x}_i) - z_i|^2 + \sum_{\mathbf{x}_i \in X_2} |f_2(\mathbf{x}_i) - z_i|^2 \tag{6}$$

with $X_1 = \{\mathbf{x}_1, \ldots, \mathbf{x}_{i'}\}$, $X_2 = \{\mathbf{x}_{i'+1}, \ldots, \mathbf{x}_k\}$ chosen a priori. As f_1, f_2 are scalar products, we re-write (6) to the cost function

$$\mathrm{GoF}(\mathbf{q}_1, \mathbf{q}_2) = \|\mathbf{C}_1\mathbf{q}_1 - \mathbf{d}_1\|^2 + \|\mathbf{C}_2\mathbf{q}_2 - \mathbf{d}_2\|^2 \tag{7}$$

where $\mathbf{C}_{1,2}$ are the monomials of $\boldsymbol{\mathcal{P}}_n(\cdot)$ evaluated in the observations of X_1 and X_2, respectively, and $\mathbf{d}_{1,2}$ are the vectors $\mathbf{d}_1 = \begin{bmatrix} z_1 & \cdots & z_{i'} \end{bmatrix}^T$, $\mathbf{d}_2 = \begin{bmatrix} z_{i'+1} & \cdots & z_k \end{bmatrix}^T$. The optimal coefficients are now subject to the unconstrained ($\mathbf{A} = \mathbf{0}$) linear-least square problem

$$\begin{bmatrix} \mathbf{q}_1 \\ \hdashline \mathbf{q}_2 \end{bmatrix} = \arg\min_{\mathbf{q}'} \left\| \left[\begin{array}{c:c} \mathbf{C}_1 & \mathbf{0} \\ \hdashline \mathbf{0} & \mathbf{C}_2 \end{array}\right] \mathbf{q}' - \begin{bmatrix} \mathbf{d}_1 \\ \hdashline \mathbf{d}_2 \end{bmatrix} \right\|_2^2 . \tag{8}$$

Here, continuity of the piecewise defined f over its entire domain holds if

$$\langle \boldsymbol{\mathcal{P}}_n(\mathbf{x}), \mathbf{q}_1 \rangle = \langle \boldsymbol{\mathcal{P}}_n(\mathbf{x}), \mathbf{q}_2 \rangle \tag{9}$$

for all $\mathbf{x} \in \Omega_\varphi$. For single-variate functions, we have value continuity for the identity function $\varphi = \mathrm{id}$ and x_0 is zero of

$$\langle \boldsymbol{\mathcal{P}}_n(x), \mathbf{q}_1 - \mathbf{q}_2 \rangle.$$

In this scheme, the observations still need to be split into X_1 and X_2 initially; however, this leaves the actual joint to be free. As the observations form a discrete set, an optimization approach over $X_{1,2}$ would be fair and just, thus yielding an ideal model. With piecewise polynomial fitting keeping most properties of polynomial regression, it has been proven numerically in [22] that the inaccuracy of a fitted erroneous signal is reduced: given data pairs $(x_i, z_i)_i$ by (4) with $\epsilon \sim \mathcal{N}(0, \sigma)$ and a piecewise fit f, the standard deviation of f to the true values, $\gamma(x) - f(x)$, is smaller than the measurement error σ.

C. Constraint matrices

As the coefficients define a polynomial uniquely, we can restrict the coefficients (i.e., the polynomials) by constraint matrices:

Proposition 1 (Constraint of continuity [22]) *Let* $\varphi(\mathbf{x}) = \mathbf{a}^T\mathbf{x} \leq x_0$ *be a linear matrix inequality (LMI) with* $\mathbf{a}^T = \begin{bmatrix} a_1 & \cdots & a_m \end{bmatrix}$ *and* $a_1 \neq 0$*; a piecewise polynomial function* f *with continuity in* Ω_φ *is subject to the constrained LSQ problem given by the continuity constraint matrix* $\boldsymbol{C}$*, i.e.,*

$$\boldsymbol{C}\begin{bmatrix} \mathbf{q}_1 \\ \\ \mathbf{q}_2 \end{bmatrix} = 0 \Longleftrightarrow \forall \mathbf{x} \in \Omega_\varphi. \quad \langle \boldsymbol{\mathcal{P}}_n(\mathbf{x}), \mathbf{q}_1 \rangle = \langle \boldsymbol{\mathcal{P}}_n(\mathbf{x}), \mathbf{q}_2 \rangle. \tag{10}$$

The constraint matrix $\boldsymbol{C}$ is constructed by separation of the constrained variables into $\boldsymbol{\Lambda}_0$ such that

$$\langle \boldsymbol{\mathcal{P}}_n(\mathbf{x}_0), \mathbf{q}_{1,2} \rangle = \langle \boldsymbol{\mathcal{P}}_n(\tilde{\mathbf{x}}), \boldsymbol{\Lambda}_0\mathbf{q}_{1,2} \rangle \tag{11}$$

for all $\mathbf{x}_0 \in \left\{ \mathbf{x} \middle| \mathbf{a}^T\mathbf{x} = x_0 \right\}$, where $\tilde{\mathbf{x}}$ are the remaining free variables; we then have that

$$\langle \boldsymbol{\mathcal{P}}_n(\tilde{\mathbf{x}}), \boldsymbol{\Lambda}_0\mathbf{q}_1 \rangle = \langle \boldsymbol{\mathcal{P}}_n(\tilde{\mathbf{x}}), \boldsymbol{\Lambda}_0\mathbf{q}_2 \rangle$$

for all $\tilde{\mathbf{x}} \in \mathbb{R}^{m-1}$ if and only if $\boldsymbol{\Lambda}_0\mathbf{q}_1 = \boldsymbol{\Lambda}_0\mathbf{q}_2$ and hence, Equation (10) holds for $\boldsymbol{C} = \begin{bmatrix} \boldsymbol{\Lambda}_0 & -\boldsymbol{\Lambda}_0 \end{bmatrix}$.

Due to measurement errors or modelling flaws, a polynomial fitting may have relations that either do not exist or shall not be modeled; e.g., for a symmetric aircraft aligned to the flow, there is no side-force—regardless its angle of attack. In this case, it is desirable to constrain the resulting polynomial to be zero (or constant) for certain parameters $\tilde{\mathbf{x}}' = \left(x_{j+1}, \cdots, x_m\right)$:

Proposition 2 (Zero constraint [22]) *Let* $\mathbf{x}' = \left(x_1, \ldots, x_j\right)$ *for* $j > 0$*; a polynomial* $f = \langle \boldsymbol{\mathcal{P}}_n(\mathbf{x}), \mathbf{q} \rangle$ *with*

$$\forall \mathbf{x}' \in \mathbb{R}^j. \quad \langle \boldsymbol{\mathcal{P}}_n\left(\mathbf{x}', \mathbf{0}_{m-j}\right), \mathbf{q} \rangle = 0 \tag{12}$$

and $\mathbf{0}_{m-j} \in \{0\}^{m-j}$ *is subject to the constrained LSQ problem given by the zero constraint matrix* $\boldsymbol{\mathcal{Z}}$*.*

D. Implementation

The approach of piecewise polynomial fitting has two major modes, namely either the joint condition is a result of fitting or the joint is chosen a priori; that is, without or with a given constraint of continuity, respectively. The main steps for both modes are illustrated by the flow chart in Fig. 1, given the split sets of parameters, $X_1 = \{\mathbf{x}_1, \ldots, \mathbf{x}_{i'}\}, X_2 = \{\mathbf{x}_{i'+1}, \ldots, \mathbf{x}_k\}$ and the corresponding observations $Z = \{z_1, \ldots, z_k\}$. Preliminary to the implementation of objective and constraints matrices, we have the computation of the monomials in $\mathbf{x}$. While the order of monomials is arbitrary for fitting, we introduce here the following convention: for $\boldsymbol{\nu}, \boldsymbol{\mu} \in \mathbb{N}^m$, the monomial $\mathbf{x}^{\boldsymbol{\nu}}$ precedes $\mathbf{x}^{\boldsymbol{\mu}}$ as element of $\boldsymbol{\mathcal{P}}_n(\mathbf{x})$ if and only if $\|\boldsymbol{\nu}\|_1 < \|\boldsymbol{\mu}\|_1$ or the first non-zero element of $(\boldsymbol{\nu} - \boldsymbol{\mu})$ is positive and $\|\boldsymbol{\nu}\|_1 = \|\boldsymbol{\mu}\|_1$. In consequence, the vector of monomials breaks up into blocks of monomials $\mathbf{x}^{\mathbf{n}}$ of equal total degree $\|\mathbf{n}\|_1 = N$, denoted by $\mathbf{p}_N \in \mathbb{R}\,[\mathbf{x}]^{\mathrm{r}[N]}$, and $N \in [0; n]$ ascending. The vector of monomials can be computed recursively for a given $\mathbf{x} \in \mathbb{R}^m$ by [22, Alg. 1]. The objective matrices $\mathbf{C}_1, \mathbf{C}_2, \mathbf{d}$ of Eq. (7) can directly be computed with the elements of X_1, X_2, and Z. Without constraints, the output coefficients $\mathbf{q}_1, \mathbf{q}_2$ are subject to the unconstrained LSQ problem of (8).

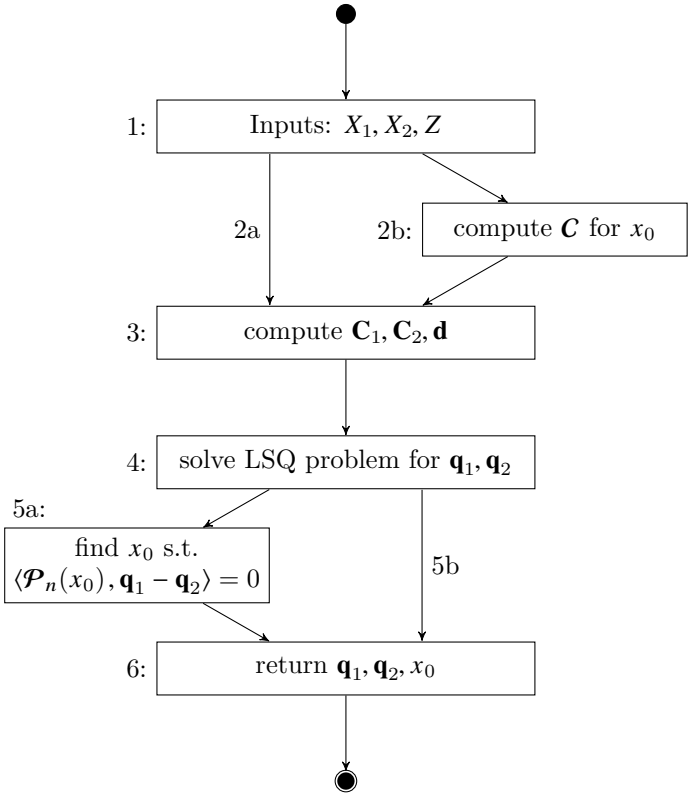

Fig. 1 Flow chart for the piecewise polynomial fitting approach: a) without continuity constraint; b) with continuity constraint in x_0.

With the definition $\boldsymbol{\mathcal{P}}_n = \begin{bmatrix} \mathbf{p}_0(\mathbf{x}) & \cdots & \mathbf{p}_N(\mathbf{x}) \end{bmatrix}$, the continuity constraint matrix $\boldsymbol{C}$ is derived from (11) by linear separation of each block. If the linear matrix inequality $\mathbf{a}^T\mathbf{x} \leq x_0$ of Proposition 1 is given with a single non-zero element of $\mathbf{a}$ – suppose, $a_1 \neq 0$ –, separation of the assigned variable $x_1 \equiv x_0$ yields

$$\mathbf{p}_N(x_0, \tilde{\mathbf{x}}) = \boldsymbol{\lambda}_N(x_0)^T\, \mathbf{p}_N(\tilde{\mathbf{x}})$$

with $\tilde{\mathbf{x}} \in \mathbb{R}^{m-1}$ and $\boldsymbol{\lambda}_N = \operatorname{diag} \mathbf{p}_N(x_0, \mathbf{1}_{m-1})$ for $\mathbf{1}_{m-1} \in \{1\}^{m-1}$. The following algorithm combines $\boldsymbol{\lambda}_0, \boldsymbol{\lambda}_1, \ldots, \boldsymbol{\lambda}_n$ into the matrix $\boldsymbol{\Lambda}_0 \sim$ `Aeq`: [22, Alg. 2]

```
one = num2cell(ones(1,m-1));
j = 0;
for N=0:n
  % let pN:=pN(·); rN:=r[N]
    pNx0 = double(pN(x0,one{:}));
    Aeq(1:rN,j+(1:rN)) = diag(pNx0);
    j = j + rN;
end
```

and $\boldsymbol{C} = \begin{bmatrix} \boldsymbol{\Lambda}_0 & -\boldsymbol{\Lambda}_0 \end{bmatrix}$. For $\mathbf{a}^T\mathbf{x} \neq x_1$, there is an invertible $\boldsymbol{\pi} : \mathbb{R}^m \to \mathbb{R}^m$ with $\mathbf{a}^T\boldsymbol{\pi}(\mathbf{y}) = y_1$ for $\mathbf{y} = (y_1, \ldots, y_m)$ [22, Lemma 7] and we thus fit polynomials $g_{1,2}$ with continuity constraint in $y_1 \equiv x_0$, resulting in

$$f_1 = \left(g_1 \circ \boldsymbol{\pi}^{-1}\right); \qquad f_2 = \left(g_2 \circ \boldsymbol{\pi}^{-1}\right).$$

The computation of the zero constraint is not illustrated in Fig. 1 but is given, regardless the constraint of continuity, by [22, Alg. 3] and precedes the solution of the LSQ problem. However, if both zero constraint and constraint of continuity are given, we need to ensure full rank of the complete constraint matrix,

$$\begin{bmatrix} \boldsymbol{C} \\ \boldsymbol{\mathcal{Z}} \end{bmatrix} \mathbf{q}' = \mathbf{0}.$$

IV. Piecewise, Full-envelope Aircraft Model

Modeling the aerodynamic coefficients of the GTM piecewise around the stall angle of attack, results in the six-degrees-of-freedom equations of motion

$$\mathbf{f}\colon (\mathbf{X},\mathbf{U}) \longmapsto \dot{\mathbf{X}} = \begin{cases} \mathbf{f}^{pre}(\mathbf{X},\mathbf{U}) & \text{if } \alpha \le \alpha_0; \\ \mathbf{f}^{post}(\mathbf{X},\mathbf{U}) & \text{else;} \end{cases} \tag{13}$$

where $\mathbf{X}$ and $\mathbf{U}$ denote the state and input vectors

$$\mathbf{X} = \begin{bmatrix} V & \alpha & \beta & \mu & \gamma & \chi & p & q & r & \Phi & \Theta & \Psi \end{bmatrix}^T$$

and $\mathbf{U} = \begin{bmatrix} \xi & \eta & \zeta & F \end{bmatrix}^T$. Here, the angles of aerodynamics (α, β), air-path (μ, γ, χ), and attitude (Φ, Θ, Ψ) are defined by the axis systems of ISO 1151-1 (Fig. 2): the *body axis system* $\left(x_f, y_f, z_f\right)$ aligned with the aircraft's fuselage; the *air-path axis system* $\left(x_a, y_a, z_a\right)$ defined by the velocity vector; and the *normal earth-fixed axis system* $\left(x_g, y_g, z_g\right)$. The air speed V is the aircraft's absolute velocity relative to the air and the body rates (p, q, r) are defined around the body axes; as usual, the control inputs are aileron, elevator, and rudder deflections ξ, η, ζ, respectively, and the thrust F.

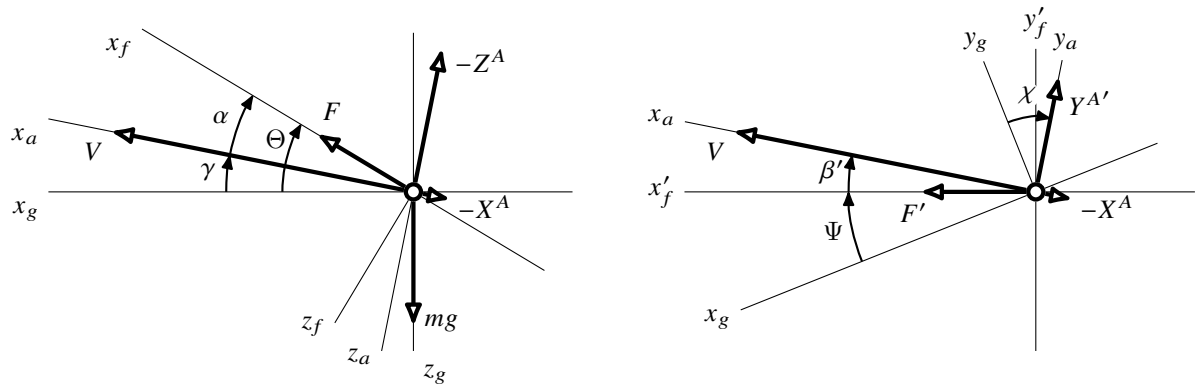

(a) Longitudinal axes ($\beta = \mu = 0$). **(b) Horizontal axes ($\gamma = 0$).**

Fig. 2 Axis systems with angles and vectors (projections into the plane are marked by $'$).

A. Equations of motion

A non-linear system of equations of motion for the six-degrees-of-freedom aircraft model of the GTM has been proposed in [25]. Here, the changes of air speed V, side-slip β, inclination γ, and azimuth χ are subject to lift, drag, thrust, and side-force (given by the aerodynamic force coefficients $C_{\mathrm{X}}, C_{\mathrm{Y}}, C_{\mathrm{Z}}$ and the thrust input F); the changes of angular body rates $\dot{p}, \dot{q}, \dot{r}$ are given by the aerodynamic moment coefficients $C_{\mathrm{l}}, C_{\mathrm{m}}, C_{\mathrm{n}}$; and the changes of attitude Φ, Θ, Ψ are functions of the angular body rates.

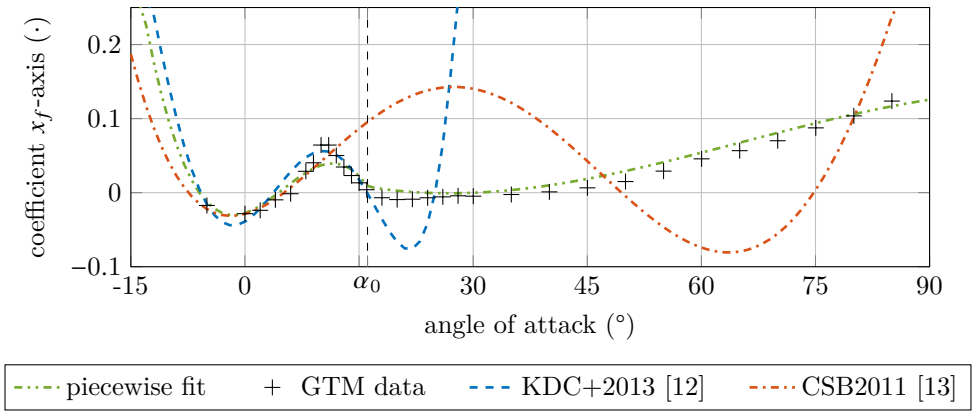

Fig. 3 Comparison of 3rd-order polynomial [10, 11] and piecewise identifications. [12]

B. Aerodynamic coefficients

The aerodynamic coefficients of the GTM are measured by its angle of attack, side-slip angle, surface deflections, and normalized body rates. [9] The measurements are given by the unknown function $\Gamma(\cdot)$:

$$\mathbf{C}_i = \Gamma(\alpha_i, \beta_i, \xi_i, \eta_i, \zeta_i, \hat{p}_i, \hat{q}_i, \hat{r}_i) + \boldsymbol{\epsilon}_i \tag{14}$$

for $i \in [1, k]$ and $\mathbf{C}_i = (C_{\mathrm{X},i}, C_{\mathrm{Y},i}, C_{\mathrm{Z},i}, C_{\mathrm{l},i}, C_{\mathrm{m},i}, C_{\mathrm{n},i})$ with $\boldsymbol{\epsilon}_i$ an unknown measurement error. Here, simple polynomial models are unsuitable to represent the full-envelope aerodynamics (Fig. 3; see also [12]). Instead, we will fit the pre-stall and post-stall dynamics piecewise to $(\mathbf{C}_i)_{1\le i\le k}$ by

$$C_\odot(\alpha, \beta, \dots) = \begin{cases} C_\odot^{pre}(\alpha, \beta, \dots) & \text{if } \alpha \le \alpha_0; \\ C_\odot^{post}(\alpha, \beta, \dots) & \text{else;} \end{cases} \tag{15}$$

and $C_\odot \in \{C_\mathrm{X}, C_\mathrm{Y}, C_\mathrm{Z}, C_\mathrm{l}, C_\mathrm{m}, C_\mathrm{n}\}$ are polynomials in the inputs to (14). Initially, a value for α_0 is found by fitting C_X with respect to the angle of attack only and solve

$$C_{\mathrm{X}\alpha}^{pre}(\alpha) = C_{\mathrm{X}\alpha}^{post}(\alpha),$$

resulting in $\alpha_0 = 16.1110°$. The obtained C_X-model as well as $(\mathbf{C}_i)_{1\le i\le k}$ are shown by Fig. 3. The boundary condition $\alpha \equiv \alpha_0$ then resembles a hyper-plane and for the full envelope, $C_\odot^{pre}$, $C_\odot^{post}$ are chosen to be sums of 3rd-order polynomials

$$C_\odot^\times = C_{\odot\alpha}^\times(\alpha) + C_{\odot\beta}^\times(\alpha, \beta) + C_{\odot\xi}^\times(\alpha, \beta, \xi) + C_{\odot\eta}^\times(\alpha, \beta, \eta) + C_{\odot\zeta}^\times(\alpha, \beta, \zeta) + C_{\odot p}^\times(\alpha, \hat{p}) + C_{\odot q}^\times(\alpha, \hat{q}) + C_{\odot r}^\times(\alpha, \hat{r}) \tag{16}$$

for $\times \in \{pre, post\}$. Continuity of the single terms at the boundary α_0,

$$C^{pre}_{\odot *}(\alpha_0, \dots) = C^{post}_{\odot *}(\alpha_0, \dots) \tag{17}$$

for all $C_{\odot *}$ and inputs, then implies continuity of (15). Lastly, we require the lateral coefficients (C_Y, C_l, C_n) vanish in the symmetric setting, i.e., zero side-slip, no aileron nor rudder deflection ($\beta = \xi = \zeta = 0$), nor out-of-plane body rates ($\hat{p} = \hat{r} = 0$). Fig. 4 shows the piecewise polynomial model of the GTM aerodynamic coefficients for angle of attack with neutral surface deflections ($\xi = \eta = \zeta = 0$) and zero body rates ($p = q = r = 0$). All functions are continuous in the joint α_0 and the lateral coefficients vanish in $\beta \equiv 0$. As only value continuity is ensured here, the obtained model is not continuously differentiable in α_0; a more general spline approach would allow for higher continuity, but comes at the cost of a priori choice of the joint. The full polynomial expressions can be found in the technical report [25].

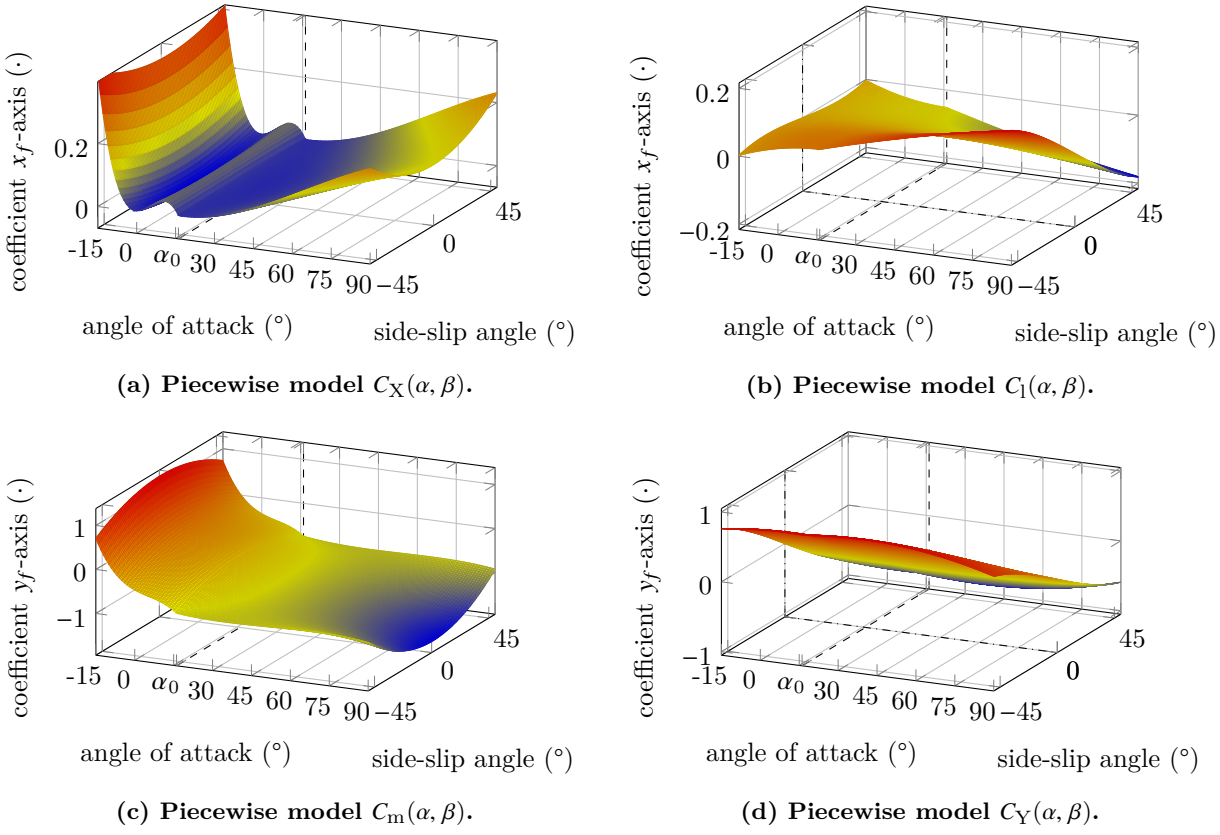

(a) Piecewise model $C_\mathrm{X}(\alpha, \beta)$.

(b) Piecewise model $C_\mathrm{l}(\alpha, \beta)$.

(c) Piecewise model $C_\mathrm{m}(\alpha, \beta)$.

(d) Piecewise model $C_\mathrm{Y}(\alpha, \beta)$.

Fig. 4 (Part 1) Piecewise model of the aerodynamic coefficients in angle of attack and side-slip angle for neutral surface deflections.

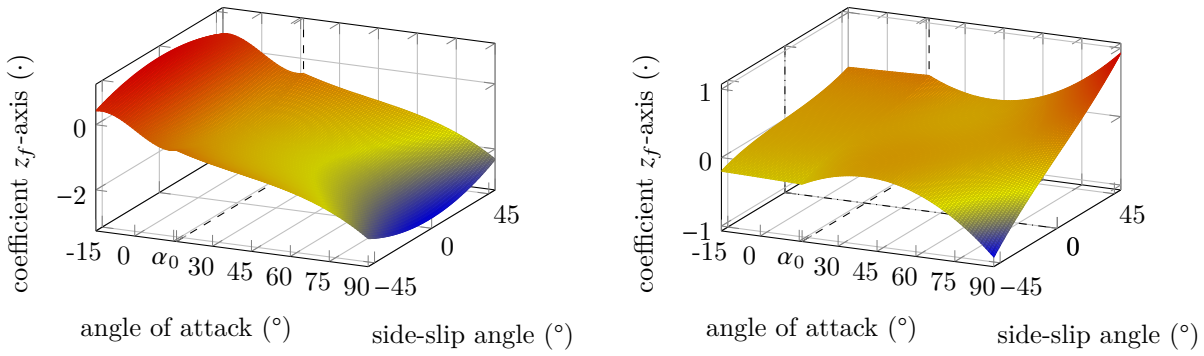

(e) Piecewise model $C_{\mathrm{Z}}(\alpha, \beta)$. **(f) Piecewise model $C_{\mathrm{n}}(\alpha, \beta)$.**

Fig. 4 (Part 2) Piecewise model of the aerodynamic coefficients in angle of attack and side-slip angle for neutral surface deflections.

V. Towards Analysis of Piecewise Models

Functional analysis of full-envelope aerodynamic models, such as continuation of trim conditions and estimation of regions of attraction, provides insight into the dynamical and statical properties of aerial systems in their extended operation range. This section provides adaptations of analysis tools used in the literature for the piecewise defined polynomial equations of motion of §IV despite the discontinuity in the first derivative around stall.

A. Trim condition analysis

The theory of continuation and bifurcation considers the equilibria of a dynamic system

$$\dot{\mathbf{X}} = \mathbf{f}(\mathbf{X}, \mathbf{U}, \boldsymbol{\mu}), \tag{18}$$

where $\boldsymbol{\mu}$ denotes the parameters of the continuation, which may include state variables and control inputs as well as other properties of $\mathbf{f}$ such as system parameters or external influences. By variation of the parameters $\boldsymbol{\mu}$ we can discuss the evolution, in particular creation, vanishing, and changes of stability, of the branches of equilibria $(\mathbf{X}^*, \mathbf{U}^*, \boldsymbol{\mu}^*)$, i.e., $\mathbf{f}(\mathbf{X}^*, \mathbf{U}^*, \boldsymbol{\mu}^*) = \mathbf{0}$, as function of $\boldsymbol{\mu}^*$. Toolboxes like the *Continuation Core and Toolboxes* (COCO) [26] offer computation of continuation and bifurcation of continuous functions. The GTM equations of motion is said to be in a *trim condition* if and only if the airspeed and air-path are constant, i.e., $\dot{V} = \dot{\gamma} = 0$; the side force vanishes, $\dot{\beta} = 0$; the body rates remain unchanged; and roll and pitch angles are constant. The heading is constant for level flight ($\dot{\Psi} = \dot{\chi} = 0$). We now choose the continuation parameters out of airspeed V, inclination γ, bank-angle μ, angle of attack α, side-slip β, the normalized rates $\hat{p}, \hat{q}, \hat{r}$, the surface deflections ζ, η, ξ, and thrust F, leaving the remaining quantities as free variables. We have now the

system of equations of motion in (18) defined piecewise as

$$\mathbf{f}(\mathbf{X},\mathbf{U},\boldsymbol{\mu}) = \begin{cases} \mathbf{f}^{pre}(\mathbf{X},\mathbf{U},\boldsymbol{\mu}) & \text{if } \alpha \leq \alpha_0; \\ \mathbf{f}^{post}(\mathbf{X},\mathbf{U},\boldsymbol{\mu}) & \text{else.} \end{cases} \tag{19}$$

For the partial derivatives of $\mathbf{f}$ are discontinuous in α_0, the COCO toolbox cannot directly compute a continuation of the piecewise system over the entire domain. Instead, we adjust the switching behaviour manually: starting from a low angle of attack, we compute equilibria of $\mathbf{f}^{pre}$ until the boundary condition $\alpha = \alpha_0$ is reached. As continuity holds at the joint,

$$\mathbf{f}^{pre}(\mathbf{X}_0^*,\mathbf{U}_0^*,\boldsymbol{\mu}_0^*) = \mathbf{f}^{post}(\mathbf{X}_0^*,\mathbf{X}_0^*,\boldsymbol{\mu}_0^*) = \mathbf{0}, \tag{20}$$

we can switch here to the dynamics of $\mathbf{f}^{post}$ without any reset and compute the high-angle of attack equilibria starting from $\left(\mathbf{X}_0^*,\mathbf{U}_0^*,\boldsymbol{\mu}_0^*\right)$ until either the limits of the continuation parameter or the boundary again is reached. In the latter case, we switch back to the low-angle of attack dynamics, and so on until finished.

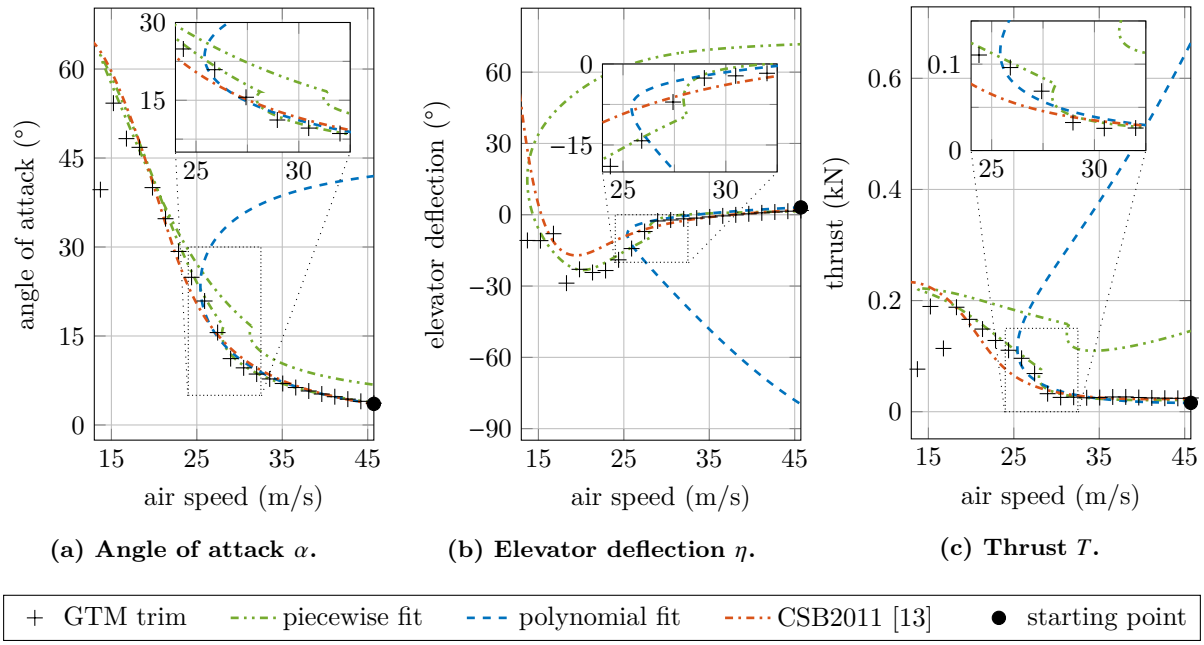

(a) Angle of attack α. **(b) Elevator deflection η.** **(c) Thrust T.**

Fig. 5 Continuation of the longitudinal dynamics of the GTM for polynomial and piecewise defined models of the aerodynamic coefficients.

In Fig. 5, we compare the piecewise continuation of (19) to polynomial models of the aerodynamic coefficients for variation of the air speed and level flight ($\gamma \equiv 0$). The polynomial model of [10] has been replaced by a similar fit. The trim data of the GTM (+) have been obtained by the trim function for the internal interpolation provided in the MATLAB simulation [9]. The first polynomial fit (- - -) shows, similar

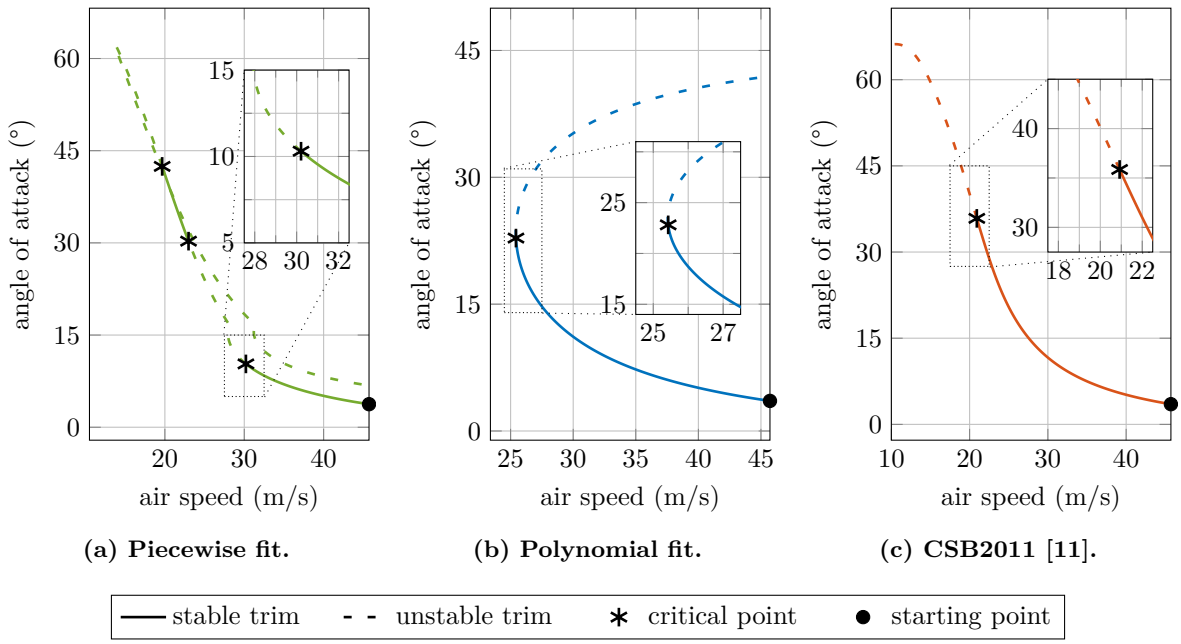

(a) Piecewise fit. **(b) Polynomial fit.** **(c) CSB2011 [11].**

Fig. 6 Stability of the longitudinal dynamics for polynomial and piecewise defined models.

to [10], a high-angle of attack branch for re-increasing air speed, which neither the polynomial fit of [11] (-·-·-) nor the piecewise fit (-·-·-) show. On the other hand, the latter certainly provide a better tracking of the GTM angle of attack, thrust, and elevator deflection values at the varying trim conditions. While for the polynomial fit of [11] the values of elevator deflection diverge to (unrealistic) multiples of 360 degrees with decreasing air speed, the elevator deflection for the piecewise fit converges, allowing a second branch of trim conditions for re-increasing air speed, too, however with far smaller angles of attack here.

We further provide in Fig. 6 information about local stability of the models: the critical point, where the trim condition changes from (locally) stable to unstable, is marked with an asterisk; stable and unstable trim conditions are drawn solid and dashed, respectively. While all three models are stable for low angles of attack and unstable for high angles, the critical points are located differently. The piecewise model shows additionally a section of stable trim conditions along the branch of increasing angles of attack, corresponding to thrust inputs larger than 135 N—i.e., 100 % throttle—and elevator deflections of −19° to −23°. Only the piecewise model has its first critical point located close to the GTM's stall angle of attack (see also Fig. 3).

B. Stable set analysis

When looking for the full-envelope, non-linear behaviour of an aircraft, knowledge about the flight envelope is vitally important for the vehicle's safety. Several characterisations of the flight envelope exist in literature. First and foremost, the desired region of the state-space can be defined by limits on the aircraft states. Within such a strict envelope, one would have the largest control-invariant set (or *safe set*) [27, 28], i.e., the largest set of initial conditions such that, given suitable control input, the aircraft is kept within the flight envelope. Finally, the regions of attraction for each stable trim condition provide a smaller, *stable set* and clearly, the safe set encapsulates the stable sets of the contained trim conditions, where every region of attraction is control-invariant in itself. While the safe set determines the abilities of the aircraft to be controlled, the stable sets highlight the limitations of a chosen controller. The neighbourhood of a trim condition $\mathbf{X}^*$ is called *stable*, denoted by $\mathcal{X}^{\text{stable}}$, if and only if for all initial conditions $\mathbf{X}_0 \in \mathcal{X}^{\text{stable}}$ the system eventually approaches $\mathbf{X}^*$. In order to compute and prove minimal stable sets of aerial vehicles based on Lyapunov function theory, researchers have successfully applied sum-of-squares programming for smooth polynomial models and ellipsoid-shaped sets [11, 29]. Given a shape $\mathcal{P}: \mathbf{X} \mapsto \mathbf{X}^T \Sigma \mathbf{X}$, Lyapunov-candidate function $\mathcal{V}$ with $\mathcal{V}(\mathbf{X}) > 0$ for all $\mathbf{X} \neq \mathbf{0}$, and $\mathbf{X}^*$ located in the origin, we have that

$$\mathcal{X}_\rho = \{\mathbf{X} \in \mathcal{X} \,|\, \mathcal{P}(\mathbf{X}) \leq \rho\} \tag{21}$$

with $\rho > 0$ is stable if and only if

$$\dot{\mathcal{V}}(\mathbf{X}) = \nabla \mathcal{V} \mathbf{f}(\mathbf{X}) < 0 \tag{22}$$

for all $\mathbf{X} \in \mathcal{X}_\rho - \{\mathbf{X}^*\}$. Equation (22) holds if there is a positive semi-definite polynomial $h \in \mathbb{R}[\mathbf{X}]$ such that

$$\nabla \mathcal{V} \mathbf{f}(\mathbf{X}) + h(\mathbf{X})\,(\rho - \mathcal{P}(\mathbf{X})) \leq -\epsilon \,\|\mathbf{X}\|_2^2, \tag{23}$$

for $\epsilon > 0$. While this technique requires continuous, polynomial functions to verify stability of a $\mathcal{X}^{\text{stable}}$, we can employ common Lyapunov function theory to compute a stable set for piecewise defined systems.

Theorem 1 ([30]) *Let $(\mathbf{f}_i)_{i \in I}$ be defined in the pair-wise disjunct $(\mathcal{X}_i)_{i \in I}$ and $\mathcal{V}(\mathbf{X}) > 0$ for all $\mathbf{X} \neq \mathbf{0}$; the neighbourhood $\mathcal{X}_\rho$ is stable if for all $i \in I$ and $\mathbf{X} \in \mathcal{X}_\rho \cap \mathcal{X}_i - \{\mathbf{0}\}$*

$$\dot{\mathcal{V}}(\mathbf{X}) = \nabla \mathcal{V} \mathbf{f}_i(\mathbf{X}) < 0. \tag{24}$$

Simply speaking, stability of $\mathcal{X}_\rho$ holds if $\dot{\mathcal{V}}$ with respect to $\mathbf{f}^{pre}$, $\mathbf{f}^{post}$ is negative just for low and high

angles of attack, respectively. Similar to (23), where $h(\mathbf{X})\,(\rho - \mathcal{V}(\cdot))$ compensates for non-negative derivatives outside the stable set, we have with positive semi-definite g_1, g_2

$$g_1(\mathbf{X})\,(\alpha_0 - \alpha) \geq 0 \Longleftrightarrow \alpha \leq \alpha_0 \tag{25}$$

$$g_2(\mathbf{X})\,(\alpha - \alpha_0) > 0 \Longleftrightarrow \alpha > \alpha_0 \tag{26}$$

and hence

$$\begin{cases} \nabla\mathcal{V}\mathbf{f}^{pre}(\mathbf{X}) + h_1(\mathbf{X})\,(\rho - \mathcal{P}(\mathbf{X})) + g_1(\mathbf{X})\,(\alpha_0 - \alpha) \leq -\epsilon\,\|\mathbf{X}\|_2^2, \\ \nabla\mathcal{V}\mathbf{f}^{post}(\mathbf{X}) + h_2(\mathbf{X})\,(\rho - \mathcal{P}(\mathbf{X})) + g_2(\mathbf{X})\,(\alpha - \alpha_0) \leq -\epsilon\,\|\mathbf{X}\|_2^2 \end{cases} \tag{27}$$

for $\epsilon > 0$ implies stability of $\mathcal{X}_\rho$ for the system of (19).

The challenge now is to find a Lyapunov function that grants a largest-possible size ρ for the chosen shape factor $\mathbf{\Sigma}$. One such approach using sum-of-squares programming is the V-s-iteration, which has been presented in [11] as iteratively-alternating steps:

1) find $\lambda^\circ = \max \lambda$ such that there is $h'(\cdot)$ positive semi-definite with

$$\nabla\mathcal{V}\mathbf{f}(\mathbf{X}) + h'(\mathbf{X})\,(\lambda - \mathcal{V}(\mathbf{X})) \leq -\epsilon\,\|\mathbf{X}\|_2^2\,;$$

2) find $\rho^\circ = \max \rho$ such that there is $h_0(\cdot)$ positive semi-definite with

$$(\mathcal{V}(\mathbf{X}) - \lambda^\circ) + h_0(\mathbf{X})\,(\rho - \mathcal{P}(\mathbf{X})) \leq 0$$

holding λ° of the first step constant;

3) find $\mathcal{V}(\cdot)$ such that

$$\begin{cases} \mathcal{V}(\mathbf{X}) \geq \quad \epsilon\,\|\mathbf{X}\|_2^2, \\ \nabla\mathcal{V}\mathbf{f}(\mathbf{X}) + h'(\mathbf{X})\,(\lambda^\circ - \mathcal{V}(\mathbf{X})) \leq -\epsilon\,\|\mathbf{X}\|_2^2, \\ (\mathcal{V}(\mathbf{X}) - \lambda^\circ) + h_0(\mathbf{X})\,(\rho^\circ - \mathcal{P}(\mathbf{X})) \leq 0, \end{cases}$$

holding $\lambda^\circ, \rho^\circ$ as well as $h'(\cdot)$ and $h_0(\cdot)$ of the previous steps constant.

Initially, a crude guess of $\mathcal{V}(\cdot)$ is found here from the linearization of $\mathbf{f}$ around $\mathbf{X}^*$ [11]. The V-s-iteration removes the difficulty to find simultaneously a Lyapunov function and its region of strictly negative time-derivative (*dissipative region*) as well as proving positive multipliers, by distinct steps of sum-of-squares

optimization. First, the dissipative region of $\mathcal{V}(\cdot)$ is determined, i.e., the level set $\mathcal{V}(\mathbf{X}) = \lambda$ such that its derivative is strictly negative within; then, the inscribing ellipsoid $\mathcal{P}(\mathbf{X}) = \rho$, the stable set, is fitted into this level set. The last step attempts to find a feasible Lyapunov function-guess with the prior results witnessing the minimal stable region. Exemplary, we compute a stable set of the piecewise model for the short-period motion,

$$\begin{bmatrix} \dot{\alpha} \\ \dot{q} \end{bmatrix} = \begin{cases} \mathbf{f}_{\mathrm{sp}}^{pre}(\alpha, q, \eta = \eta^*) & \text{if } \alpha \leq \alpha_0; \\ \mathbf{f}_{\mathrm{sp}}^{post}(\alpha, q, \eta = \eta^*) & \text{else;} \end{cases} \tag{28}$$

in the neighbourhood of the trim condition $V^* = 45.7\,\mathrm{m/s}$, $\gamma^* = 0$, $\alpha^* = 3.75°$, $\eta^* = 1.49°$, and $F^* = 21.44\,\mathrm{N}$ with the shape factor

$$\Sigma = \mathrm{diag}(20°,\, 50\,°/\mathrm{s})^{-2}$$

accounting for the physical operation range of the Generic Transport Model at the selected trim condition.

As in [11], the states have thus been scaled by the shape; the non-polynomial operations sin, cos, and $(\cdot)^{-1}$ have been replaced by finite Taylor series expansions; and polynomial terms of 6th order or higher or with coefficients absolute smaller than 10^{-6} were removed. After 94 iterations, we obtain the stable set $\mathcal{X}_{\rho 0} = \{\mathbf{X} \,|\, \mathcal{P}(\mathbf{X}) \leq \rho_0\}$ with

$$\rho_0 = 1.4404 \tag{29}$$

and the dissipative region $\{\mathbf{X} | \mathcal{V}_0(\mathbf{X}) \leq \lambda_0\} \subseteq \left\{\mathbf{X} \middle| \dot{\mathcal{V}}_0(\mathbf{X}) < 0\right\}$ of the quartic Lyapunov function $\mathcal{V}_0(\cdot)$ with

$$\lambda_0 = 0.3265. \tag{30}$$

Fig. 7 shows the stable set as well as the dissipative region of the computed common Lyapunov function. For the polynomial short-period model of [11], the stable set $\mathcal{X}_{\rho\mathrm{Pol}}$ and the respective level set of the quartic Lyapunov function $\mathcal{V}_{\mathrm{Pol}}$ have been computed to $\rho_{\mathrm{Pol}} = 1.6785$ and $\lambda_{\mathrm{Pol}} = 0.8522$, respectively, and are too shown by Fig. 7 for comparison. The obtained Lyapunov functions are given by

$$\begin{aligned} \mathcal{V}_0 = {} & 6.5\alpha^4 + 0.37\alpha^3 q + 0.19\alpha^2 q^2 + 0.023\alpha q^3 + 0.0027 q^4 - 0.080\alpha^3 \\ & + 0.000\,44\alpha^2 q + 0.012\alpha q^2 - 0.0067 q^3 + 0.69\alpha^2 - 0.016\alpha q + 0.020 q^2 \end{aligned} \tag{31}$$

and

$$\mathcal{V}_{\mathrm{Pol}} = 20\alpha^4 - 2.8\alpha^3 q + 1.6\alpha^2 q^2 - 0.21\alpha q^3 + 0.029 q^4 + 0.0033\alpha^3 + 0.000\,88\alpha^2 q$$
$$+ 0.000\,13\alpha q^2 - 2.5\times 10^{-6} q^3 + 2.6\times 10^{-5}\alpha^2 + 3.2\times 10^{-7}\alpha q + 1.4\times 10^{-6} q^2$$

It is thus demonstrated that the extension to common Lyapunov functions for the estimation of stable sets for the piecewise polynomial model is feasible using sum-of-squares programming.

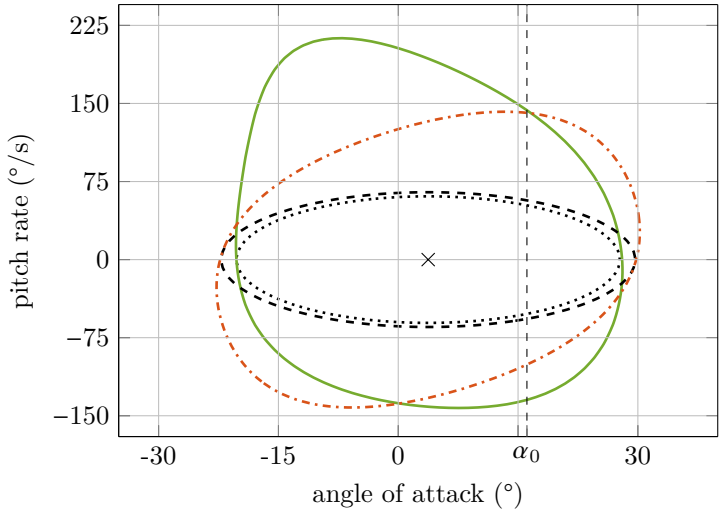

Fig. 7 Stable set of the piecewise short-period model compared to [11].

VI. Conclusion

In-flight loss-of-control remains a severe threat to civil aviation safety. In the presence of highly non-linear, unstable dynamics in upset situations, accurate models of the full-envelope aerodynamics are crucial for successful analysis, protection, and recovery of the aircraft. This note proposes piecewise polynomial fitting of the aerodynamic coefficients with a single non-smooth joint representing the change of dynamics at high angles of attack. This approach yields a model almost as simple as polynomials but with the power of splines to account for complex characteristics. The joint of the piecewise model is justified by the physical properties of the aerial system and has been subject to the fit, too. Without the necessity of a priori choices regarding the fit, we maintain all abilities of polynomial fitting. Given the example of the Generic Transport Model, we have compared the piecewise model of the aerodynamic coefficients to polynomial models available in the literature, proving the accuracy of both piecewise coefficients and trim conditions when measured

against the GTM's raw data. Functional analysis tools such as continuation of equilibria and estimation of safe and stable sets yield invaluable preparations for flight control schemes over the full envelope. We have demonstrated how those tools, typically requiring continuous inputs, can be adapted to piecewise defined systems, retaining crucial information about stability and attraction. Although the extensions apply to all kinds of piecewise models including splines, the problem size grows with the number of cases and, in particular for sum-of-squares programming, computationally unfeasible. The piecewise polynomial model for low and high angles attack, however, provides all three accuracy, regression of measurements, and feasibility of the subsequent analysis.

Funding Sources

This work is funded by ONERA – The French Aerospace Lab, République Française.

References

[1] Goman, M., Zagainov, G., and Khramtsovsky, A., "Application of bifurcation methods to nonlinear flight dynamics problems," *Progress in Aerospace Sciences*, Vol. 33, No. 9–10, 1997, pp. 539–586. doi:10.1016/S0376-0421(97)00001-8.

[2] Gill, S. J., Lowenberg, M. H., Neild, S. A., Krauskopf, B., Puyou, G., and Coetzee, E., "Upset Dynamics of an Airliner Model: A Nonlinear Bifurcation Analysis," *Journal of Aircraft*, Vol. 50, No. 6, 2013, pp. 1832–1842. doi:10.2514/1.C032221.

[3] Chang, B.-C., Kwatny, H. G., Ballouz, E. R., and Hartmann, D. C., "Aircraft Trim Recovery from Highly Nonlinear Upset Conditions," *AIAA Guidance, Navigation, and Control Conference*, San Diego, US-CA, 2016. doi:10.2514/6.2016-0880.

[4] Stepanyan, V., Krishnakumar, K., Kaneshige, J., and Acosta, D., "Stall Recovery Guidance Algorithms Based on Constrained Control Approaches," *AIAA Guidance, Navigation, and Control Conference*, San Diego, US-CA, 2016. doi:10.2514/6.2016-0878.

[5] Engelbrecht, J. A. A., Pauck, S. J., and Peddle, I. K., "A Multi-mode Upset Recovery Flight Control System for Large Transport Aircraft," *AIAA Guidance, Navigation, and Control Conference*, Boston, US-MA, 2013. doi:10.2514/6.2013-5172.

[6] Crespo, L. G., Kenny, S. P., Cox, D. E., and Murri, D. G., "Analysis of Control Strategies for Aircraft Flight Upset Recovery," *AIAA Guidance, Navigation, and Control Conference*, Minneapolis, US-MN, 2012. doi:10.2514/6.2012-5026.

[7] Richards, N. D., Gandhi, N., Bateman, A. J., Klyde, D. H., and Lampton, A. K., "Vehicle Upset Detection and

Recovery for Onboard Guidance and Control," *Journal of Guidance, Control, and Dynamics*, Vol. 40, No. 4, 2017, pp. 920–933. doi:10.2514/1.G001738.

[8] Frink, N. T., Murphy, P. C., Atkins, H. L., Viken, S. A., Petrilli, J. L., Gopalarathnam, A., and Paul, R. C., "Computational Aerodynamic Modeling Tools for Aircraft Loss of Control," *Journal of Guidance, Control, and Dynamics*, Vol. 40, No. 4, 2017, pp. 789–803. doi:10.2514/1.G001736.

[9] "Flight Dynamics Simulation of a Generic Transport Model," , 2016. URL `https://software.nasa.gov/software/LAR-17625-1`.

[10] Kwatny, H. G., Dongmo, J.-E. T., Chang, B.-C., Bajpai, G., Yasar, M., and Belcastro, C., "Nonlinear Analysis of Aircraft Loss of Control," *Journal of Guidance, Control, and Dynamics*, Vol. 36, No. 1, 2013, pp. 149–162. doi:10.2514/1.56948.

[11] Chakraborty, A., Seiler, P., and Balas, G. J., "Nonlinear region of attraction analysis for flight control verification and validation," *Control Engineering Practice*, Vol. 19, No. 4, 2011, pp. 335–345. doi:10.1016/j.conengprac.2010.12.001.

[12] Cunis, T., Burlion, L., and Condomines, J.-P., "Piece-wise Identification and Analysis of the Aerodynamic Coefficients, Trim Conditions, and Safe Sets of the Generic Transport Model," *AIAA Guidance, Navigation, and Control Conference*, Kissimmee, US-FL, 2018. doi:10.2514/6.2018-1114.

[13] Bulka, E., and Nahon, M., "Autonomous control of agile fixed-wing UAVs performing aerobatic maneuvers," *2017 International Conference on Unmanned Aircraft Systems*, Miami, US-FL, 2017, pp. 104–113. doi:10.1109/ICUAS.2017.7991437.

[14] Robison, D. E., "Estimates for the Points of Intersection of Two Polynomial Regressions," *Journal of the American Statistical Association*, Vol. 59, No. 305, 1964, pp. 214–224. doi:10.2307/2282870.

[15] Gallant, A. R., and Fuller, W. A., "Fitting segmented polynomial regression models whose join points have to be estimated," *Journal of the American Statistical Association*, Vol. 68, No. 341, 1973, pp. 144–147. doi:10.2307/2284158.

[16] McGee, V. E., and Carleton, W. T., "Piecewise Regression," *Journal of the American Statistical Association*, Vol. 65, No. 331, 1970, pp. 1109–1124. doi:10.2307/2284278.

[17] Chaudhuri, P., Huang, M.-C., Loh, W.-Y., and Yao, R., "Piecewise-Polynomial Regression Trees," *Statistica Sinica*, Vol. 4, No. 1, 1994, pp. 143–167. URL `http://www.jstor.org/stable/24305278`.

[18] de Visser, C. C., Mulder, J. A., and Chu, Q. P., "A Multidimensional Spline-Based Global Nonlinear Aerodynamic Model for the Cessna Citation II," *AIAA Atmospheric Flight Mechanics Conference*, Toronto, CA, 2010. doi:10.2514/6.2010-7950.

[19] Tol, H. J., de Visser, C. C., Sun, L. G., van Kampen, E., and Chu, Q. P., "Multivariate Spline-Based Adaptive Control of High-Performance Aircraft with Aerodynamic Uncertainties," *Journal of Guidance, Control, and Dynamics*, Vol. 39, No. 4, 2016, pp. 781–800. doi:10.2514/1.G001079.

[20] de Visser, C. C., Chu, Q. P., and Mulder, J. A., "A new approach to linear regression with multivariate splines," *Automatica*, Vol. 45, No. 12, 2009, pp. 2903–2909. doi:10.1016/j.automatica.2009.09.017.

[21] Brandon, J. M., and Morelli, E. A., "Real-Time Onboard Global Nonlinear Aerodynamic Modeling from Flight Data," *Journal of Aircraft*, Vol. 53, No. 5, 2016, pp. 1261–1297. doi:10.2514/1.C033133.

[22] Cunis, T., "The pwpfit Toolbox for Polynomial and Piece-wise Polynomial Data Fitting," *18th IFAC Symposium on System Identification*, Stockholm, SE, 2018. doi:10.1016/j.ifacol.2018.09.204.

[23] Stigler, S. M., "Gergonne's 1815 paper on the design and analysis of polynomial regression experiments," *Historia Mathematica*, Vol. 1, 1974, pp. 431–439. doi:10.1016/0315-0860(74)90033-0.

[24] Smith, K., "On the Standard Deviations of Adjusted and Interpolated Values of an Observed Polynomial Function and its Constants and the Guidance they give Towards a Proper Choice of the Distribution of Observations," *Biometrika*, Vol. 12, No. 1/2, 1918. doi:10.2307/2331929.

[25] Cunis, T., Burlion, L., and Condomines, J.-P., "Piecewise Polynomial Model of the Aerodynamic Coefficients of the Generic Transport Model and its Equations of Motion," Tech. rep., ONERA – The French Aerospace Lab; French Civil Aviation School, Toulouse, FR, 2018. URL `https://hal.archives-ouvertes.fr/hal-01808649`.

[26] Dankowicz, H., and Schilder, F., *Recipes for Continuation*, Computational Science & Engineering, Society for Industrial and Applied Mathematics, Philadelphia, US-PA, 2013. doi:10.1137/1.9781611972573.

[27] Lygeros, J., "On reachability and minimum cost optimal control," *Automatica*, Vol. 40, No. 6, 2004, pp. 917–927. doi:10.1016/j.automatica.2004.01.012.

[28] Nabi, H. N., Lombaerts, T., Zhang, Y., van Kampen, E., Chu, Q. P., and de Visser, C. C., "Effects of Structural Failure on the Safe Flight Envelope of Aircraft," *Journal of Guidance, Control, and Dynamics*, Vol. 41, No. 6, 2018, pp. 1257–1275. doi:10.2514/1.G003184.

[29] Tedrake, R., Manchester, I. R., Tobenkin, M., and Roberts, J. W., "LQR-trees: Feedback Motion Planning via Sums-of-Squares Verification," *The International Journal of Robotics Research*, Vol. 29, No. 8, 2010, pp. 1038–1052. doi:10.1177/0278364910369189.

[30] Johansson, M., and Rantzer, A., "Computation of piecewise quadratic Lyapunov functions for hybrid systems," *IEEE Transactions on Automatic Control*, Vol. 43, No. 4, 1998, pp. 555–559. doi:10.1109/9.664157.